Damage Development in Confined Borosilicate and Soda-Lime Glasses

Kathryn A. Dannemann[1], Charles E. Anderson, Jr.[1], Sidney Chocron[1], James F. Spencer[2]
[1]Engineering Dynamics Department, Southwest Research Institute, San Antonio, TX 78238,USA
[2]Materials Engineering Department, Southwest Research Institute, San Antonio, TX 78238, USA

Abstract

Post-test microscopy evaluations were performed on borosilicate (Borofloat® 33) and soda-lime (Starphire®) glass specimens following confined compression tests. These included optical and electron microscopy investigations of select specimens tested at low strain rates with confinement pressures up to 1 GPa. Specimens were evaluated following removal of the confinement sleeve or holder. The objective of this work was to investigate the flow and failure behavior of both glasses due to compressive loading with confinement. The observations provide insight into the damage process that occurs during projectile impact/penetration into transparent armor. Highlights of the microscopy evaluations are compared and contrasted for the two glasses of interest. A damage mechanism is proposed based on comparison of the mechanical response data with the post-test microscopy findings.

1. Corresponding author: kdannemann@swri.org

Report Documentation Page

Form Approved
OMB No. 0704-0188

1. REPORT DATE	2. REPORT TYPE	3. DATES COVERED
11 JUL 2011	**Technical Report**	**11-07-2011 to 11-07-2011**

4. TITLE AND SUBTITLE	5a. CONTRACT NUMBER
DAMAGE DEVELOPMENT IN CONFIRMED BOROSILICATE AND SODA-LIME GLASSES	**w56hzv-6-c-0194**
	5b. GRANT NUMBER
	5c. PROGRAM ELEMENT NUMBER
6. AUTHOR(S)	5d. PROJECT NUMBER
Kathryn Dannemann; Charles Anderson; Sidney Chocron; James Spencer	5e. TASK NUMBER
	5f. WORK UNIT NUMBER
7. PERFORMING ORGANIZATION NAME(S) AND ADDRESS(ES)	8. PERFORMING ORGANIZATION REPORT NUMBER
Southwest Research Institute,P. O. Drawer 28510,San Antonio,TX,78228-0510	**; #21945**
9. SPONSORING/MONITORING AGENCY NAME(S) AND ADDRESS(ES)	10. SPONSOR/MONITOR'S ACRONYM(S)
U.S. Army TARDEC, 6501 E.11 Mile Rd, Warren, MI, 48397-5000	**TARDEC**
	11. SPONSOR/MONITOR'S REPORT NUMBER(S)
	#21945

12. DISTRIBUTION/AVAILABILITY STATEMENT

Approved for public release; distribution unlimited

13. SUPPLEMENTARY NOTES

14. ABSTRACT

Post-test microscopy evaluations were performed on borosilicate (Borofloat? 33) and sodalime (Starphire?) glass specimens following confined compression tests. These included optical and electron microscopy investigations of select specimens tested at low strain rates with confinement pressures up to 1 GPa. Specimens were evaluated following removal of the confinement sleeve or holder. The objective of this work was to investigate the flow and failure behavior of both glasses due to compressive loading with confinement. The observations provide insight into the damage process that occurs during projectile impact/penetration into transparent armor. Highlights of the microscopy evaluations are compared and contrasted for the two glasses of interest. A damage mechanism is proposed based on comparison of the mechanical response data with the post-test microscopy findings.

15. SUBJECT TERMS

16. SECURITY CLASSIFICATION OF:			17. LIMITATION OF ABSTRACT	18. NUMBER OF PAGES	19a. NAME OF RESPONSIBLE PERSON
a. REPORT	b. ABSTRACT	c. THIS PAGE			
unclassified	**unclassified**	**unclassified**	**Same as Report (SAR)**	**34**	

1.0 Introduction

The strength of glass and other brittle materials increases with pressure. This pressure dependency is well documented for various materials, ranging from ceramics [1] to geologic materials [2]. The response of glass to a projectile/penetrator impact requires understanding of the glass response under high pressure and shear stress. Although this topic has been the subject of numerous recent publications [3-7], improved understanding of the damage development process is necessary to aid with development of more accurate constitutive models. Such models can then be applied in design efforts to enhance ballistic performance through material and geometric arrangement of armor elements. Further insight into the pressure-dependent response of glass is critical for more effective design and development of transparent armor systems.

The effects of pressure/shear have been investigated in our laboratory using non-ballistic experiments. Compression experiments are performed on confined specimens using either hydraulic or mechanical confinement. Specimens are pre-damaged and then loaded and reloaded to comminute the material. We have applied this technique previously to evaluate the effects of pressure on the damage response of ceramics [8]. The experimental data obtained were used to improve the Johnson-Holmquist constitutive model [9] for ceramics.

Other non-ballistic experiments have also been developed recently to improve understanding of the damage process and aid with modeling efforts. Shockey and colleagues [10,11] developed a test methodology to investigate the failure physics of projectile impact into thick (2-inch) borosilicate glass targets. They employed low-velocity ballistic experiments to evaluate the flow region under the penetrator. A new laboratory compression/shear experiment was devised by Nie, et al. [12] to evaluate the dynamic failure of glass. A modified version of the split

Hopkinson (Kolsky) bar is used to generate a shear stress component in cuboid test specimens oriented at different angles to the loading direction. Experimental results for borosilicate glass show that the equivalent stress at failure decreases as the shear component of the stress increases. Chen, et al. [13,14] also developed a Hopkinson bar technique that utilizes double pulse loading to better simulate an impact event for a brittle material (e.g. ceramics or glasses). The first pulse determines the dynamic response of the intact material and then crushes the specimen; the second pulse determines the dynamic compressive response of a damaged material with interlocking pieces. A ring-on-ring technique was used by Wereszczak, et al. [15] to investigate contact damage for soda-lime and borosilicate glasses. Similar experiments were implemented at high strain rates using a Hopkinson bar setup [16].

Post-test microscopy investigations have been applied to better understand the damage development process. Shockey [10,11] evaluated the flow region under the penetrator in impacted targets of borosilicate glass. Some melting was observed on glass adhered to the projectile. Bless [17] investigated multilayered glass targets following projectile impact and documented the damage regions in individual layers. Nie and Chen [14] studied the effects of temperature and confinement pressure on the dynamic response of damaged borosilicate glass. Dannemann [18,19] evaluated the progression of damage and the effects of increasing confinement pressure using interrupted laboratory compression tests for glass specimens with mechanical confinement.

The objective of the present work was to investigate the flow and failure behavior of glass under confinement. This includes investigation of failure along observed shear planes. Borofloat and Starphire glass specimens were tested in confined compression under quasistatic loading. Several tests were also performed at higher strain rates (~1 s^{-1} to 1000 s^{-1}).

Confinement sleeves/holders were removed following testing and specimens evaluated using optical and electron microscopy. This work expands on prior work by the authors [18,19] where the onset and extent of damage in Borofloat glass were evaluated.

2.0 Materials

Borofloat®33 (BF) and Starphire® (SP) glasses were evaluated. Both glasses were obtained from Swift Glass (Elmira, NY). BF is a borosilicate glass manufactured by Schott Glass using a float process. SP float glass is a crystal clear, soda-lime glass. This low Fe, low Pb glass, manufactured by Pittsburgh Plate Glass (PPG), has a more consistent composition than ordinary soda-lime glass with similar physical and mechanical properties. Compositions of the two glasses are summarized in Table 1; these were determined from X-ray fluorescence analysis [20]. Both glasses also contain minor amounts of other oxides not included in the table. The high transparency of the BF and SP glasses, and the clear edge characteristics of the SP glass, is related to their low Fe content.

Properties of the BF and SP glasses were measured using an ultrasonic technique (ASTM E494[21]); the results are summarized in Table 2. The elastic modulus and Poisson's ratio determined from ultrasonic measurements are similar to those measured from the compression experiments. The density and Poisson's ratio, and elastic and shear moduli, are lower for BF vs. SP glass. The linear coefficient of thermal expansion for each glass is also included for comparison. These values were obtained from the manufacturer technical datasheets [22,23]. The thermal expansion coefficient for BF glass is approximately one third the value for SP glass.

Ceramic anvils, positioned between the test specimen and the loading platens, were used to load the confined specimens during compression testing. Initial tests were performed with

tapered tungsten carbide loading anvils; subsequent confined sleeve tests utilized higher strength SiC-N anvils. Tapered alumina (AD-995) anvils were used for the hydraulic confinement experiments. The annular confining sleeves for the mechanical confinement tests were fabricated from maraging steel, Vascomax C350, to maximize confinement pressure without yielding the confining sleeve.

3.0 Experimental Procedure

3.1 Specimen Preparation

The compression experiments were performed on polished cylindrical glass test specimens with a length:diameter ratio of 2. The specimens were ground from plate, and measured 6.35-mm in diameter and 12.7-mm long. Owing to the inherent flaw sensitivity of glass, all specimens were polished to a high-end optical finish (80/50 scratch-dig) to minimize surface defects. Flatness and parallelism of the specimen ends, especially critical when testing brittle materials, were maintained to within 0.005-mm.

Both intact and pre-damaged specimens were evaluated. Test specimens were pre-damaged using a thermal shock technique. The thermal shock procedure consisted of two 0.3-h exposures at 500°C in a resistance tube furnace, followed by an ice water quench after each thermal exposure. The procedure was applied to individual test specimens, rather than exposing multiple specimens at once. The thermal shock treatment was sufficient to pre-damage the glass specimens while maintaining specimen integrity such that specimens could be handled during test preparations without imparting further damage. Stereomicroscopy evaluations of the thermally shocked samples were performed prior to confinement testing to evaluate the extent of damage. A consistent damage pattern was observed for each glass. Representative damage

patterns are illustrated in Figure 1. The damage pattern for the BF glass (Figure 1a) shows a limited number of very distinct cracks; SP glass (Figure 1b) exhibits a network of interconnected cracks. The damage pattern and extent differs, although the same thermal shock procedure was employed.

3.2 Confined Compression Tests

Most compression experiments were conducted at quasistatic strain rates ($\sim 10^{-3}$ s^{-1}). Several tests were also performed at higher strain rates to assess strain rate dependence. These were conducted on pre-damaged specimens using a Hopkinson (Kolsky) bar setup. The quasistatic and intermediate rate (~ 1 s^{-1}) tests were conducted using an MTS servohydraulic machine. Specimens were confined using either a mechanical or hydraulic confinement technique.

With the hydraulic confinement technique, a constant confinement pressure is maintained during testing. The hydraulic confinement test is a triaxial compression test, commonly used to characterize pressure-dependent materials (e.g., sand or concrete) [2,24]. A maximum confinement pressure of 500 MPa is possible with our current setup. Tests were performed at fluid pressures of 25, 50, 100, 250, 400, and 500 MPa. Each glass specimen was placed in a Teflon shrink tube sleeve for protection from the hydraulic fluid. A piston was used to load the specimen inside the pressure vessel using two ceramic anvils. The load was measured with a load cell placed inside the pressure vessel and wired directly to provide the equivalent stress acting on the specimen. The axial strain in the specimen was measured using a calibrated extensometer.

For mechanical confinement, a 3.2-mm thick high-strength steel sleeve was used to confine the specimen during testing. Individual confining sleeves were honed to fit each test specimen,

and minimize the clearance between the test specimen and the inner diameter of the sleeve. The sleeved specimens were loaded in displacement control. The confinement pressure changes during compressive loading of the sleeved specimen, and is dependent on the extent of loading. The maximum confining pressure achieved was approximately 1 GPa. Load was measured with the load cell on the MTS loadframe. Axial strains in the specimen were measured with an extensometer, with arms situated on the loading platens. Strain gages, mounted on the mid-section of the confining sleeve, were also used to measure axial and hoop strains in the sleeve. Additional details for the confined compression experiments and techniques are described in Refs. [8,18,25].

3.3 Post-Test Specimen Evaluation

Specimens were evaluated to determine the extent of damage, with increasing load and pressure levels, and the extent of failure. Careful specimen preparation and handling was necessary to ensure the fracture/failure characteristics were captured without imparting further damage to the specimens, or disrupting loose or interlocking glass fragments.

Initial investigations were performed with optical and stereomicroscopy. Higher resolution microscopy, using a scanning electron microscope (SEM), was performed on select BF and SP specimens with damage features of interest. These were selected based on the optical microscopy evaluations. The SEM investigations were implemented to provide more detailed analyses in the vicinity of the dominant shear plane, including the morphology of the glass fragments along the resulting shear plane. SEM evaluations required application of a gold coating to the glass specimens to limit specimen charging under the electron beam.

To view the damage *in-situ*, it was necessary to remove the steel sleeve or Teflon holder around the specimen. The technique for removing a section of the steel confinement sleeve was perfected in previous investigations [18]. A longitudinal section of the steel sleeve was carefully removed to minimize disturbance to the tested specimen. Removal of a "pie section" from the steel sleeve, as shown in Figure 2a, allowed viewing of *in-situ* damage along the entire specimen length. Internal damage was readily visible owing to the transparency of the glass. Cutting of the steel sleeve was initially performed with a Dremel tool; electro-discharge machining (EDM) was implemented subsequently to obtain precision cuts with minimal specimen damage. Numerous confined sleeve specimens were evaluated, as the location of the opening did not always correspond with the dominant shear plane location.

For specimens tested in triaxial compression, slitting and opening of the Teflon sleeve, and underlying brass foil, was necessary to view specimen damage. The thin brass foil was wrapped around the specimen to prevent damage to the Teflon shrink tubing due to fragmentation of the glass during testing. Perfection of the cutting/opening technique was required to minimize further damage to the specimen. If the position of the anvils within the Teflon sleeve was not maintained during the sectioning process, shifting and disruption of glass fragments along the shear plane occurred. Figure 2b shows a BF specimen tested in triaxial compression following cutting and opening of the shrink tube.

4.0 Results

Axial stress vs. axial strain curves were obtained for each confined compression test. For the confined sleeve tests, axial stress vs. hoop strain plots were also obtained. The axial stress-strain response of intact and pre-damaged BF and SP glass are compared in Figure 3 for

specimens tested with hydraulic confinement; confinement pressures are included on the plot. Each curve corresponds to a single test, and is representative of the behavior of each glass at similar confinement pressures. The response differs for intact vs. predamaged glass, but is consistent for BF and SP glass.

The axial stress-strain curves for *intact* confined glass follow a similar trajectory. The failure stress for the intact glass increases with confining pressure. The stress-strain curves for the intact glasses are generally linear until failure. Failure occurs suddenly as indicated by the vertical arrows in Figure 3. Some deviation from linearity is evident for the intact BF glass. The cause of the non-linearity was not investigated, but may be related to densification of the glass. Densification of BF glass has been demonstrated in recent work by Holmquist and Johnson [3].

The *predamaged* glass exhibits a dramatic response difference vs. the intact specimens. A linear stress-strain response was measured upon initial loading of the confined, predamaged specimens. The moduli are less than for the corresponding intact specimens, owing to the presence of cracks in the predamaged specimens. With continued loading, a maximum axial stress is reached; this stress is lower than the failure strength of the corresponding intact glass. The strength then drops to a lower value which is maintained with increasing axial strain, as shown in Figure 3. This indicates load carrying capability even after initial damage occurs. Previous interrupted tests on BF glass specimens with mechanical confinement showed specimen strength was maintained until a critical stress level was exceeded [19]. The residual strength values shown in Figure 3 vary with the confinement pressure; higher confining pressure corresponds to higher residual strength. Similar residual strengths were measured for BF and SP glass at each confinement pressure tested. The fluctuation in the curves around the residual strength value likely occurs due to particle movement and extension of pre-existing cracks, as

discussed in the next section. Additional details on the mechanical response are provided in recent publications [25,26].

Experimental data from both types of tests were reduced to equivalent stress versus pressure plots for direct performance comparisons of the two glasses, and to assess the effect of specimen condition (e.g., intact, pre-damaged) on response. The equivalent stress, for axial symmetry, is defined by:

$$\sigma_{eq} = | \sigma_z - \sigma_r | = \tilde{\sigma}_z - \tilde{\sigma}_r \tag{1}$$

where σ_z is the axial load and σ_r is the radial load. For the triaxial compression tests, σ_r is the fluid pressure from the hydraulic confinement ($\sigma < 0$ in compression, $\tilde{\sigma} > 0$ in compression). For the confined sleeve tests, σ_r is determined analytically based on the hoop strain in the steel sleeve – assuming the sleeve remains elastic [25]. The pressure for the equivalent stress vs. pressure plots is the hydrostatic pressure derived from the confining pressure. The hydrostatic pressure on the specimen is given by Eqn (2). See Chocron, et al. [25] for details of the analysis.

$$P = \frac{1}{3}(2\tilde{\sigma}_r + \tilde{\sigma}_z) \tag{2}$$

Maximum equivalent stress vs. hydrostatic pressure comparison plots for intact and pre-damaged glass are shown in Figures 4 and 5, respectively. The behavior of confined vs. unconfined *intact* glass is compared in Figure 4 for BF and SP glass. The equivalent stress versus pressure response for *intact*, unconfined glass lies on a line with a slope of 3, from Eqn. (1) and (2) since $\tilde{\sigma}_r = 0$ for the unconfined tests. There is considerable scatter in the intact strength of both glasses, though BF glass is generally stronger than SP glass. The strength (i.e., equivalent stress) increases with confinement, while the scatter in the intact strength decreases with confinement.

The confined compression test results for *pre-damaged* BF and SP glasses are shown in Figure 5. Both predamaged glasses exhibit similar behavior, and strength, at hydrostatic pressures less than ~1 GPa (the pressure range for the predamaged data in Figure 3). The difference becomes more pronounced at higher pressures: greater than 1.0 GPa and 1.2 GPa for SP and BF glass, respectively. When the hydrostatic pressure exceeds a critical pressure, a strength cap occurs. Pre-damaged SP glass exhibits a strength cap at approximately 1.6 GPa. The strength of the pre-damaged BF glass continues to increase until reaching an approximate equivalent stress of 2.1 GPa. Figure 5 shows the strength cap is approximately 0.5 GPa higher for BF glass. The residual strength difference between the BF and SG glass may help to explain recent findings by Bless [27] where BF glass demonstrated greater penetration resistance vs. SP glass in depth of penetration experiments using both blunt and sharp projectiles.

5.0 Discussion

The slopes of the equivalent stress vs. pressure plots in Figures 4 and 5 are independent of the damage condition (i.e., intact vs. predamaged). However, the intercept varies with the extent of damage. The lower residual strength of predamaged SP glass (vs. predamaged BF glass), shown in Figure 5, may be related to the higher level of initial damage for SP glass (see Figure 1). Predamaged SP glass specimens exhibited an extensive network of interconnected cracks. The lower thermal shock resistance and more extensive cracking for the SP glass is attributed to its high linear expansion coefficient (3x greater than BF glass).

The difference in response for the unconfined intact glasses, shown in Figure 4, demonstrates an inherent compositional difference between SP and BF glass. Compositional differences may also indirectly affect the maximum strength (cap) of the predamaged glass.

5.1 Post-Test Microscopy Observations

Axial loading of both glasses, whether intact or pre-damaged, results in formation of a dominant shear plane. Damage likely initiates from flaws and/or pre-existing cracks due to the thermal shock procedure. Compression loading of the specimen causes slippage, and movement of the material. For BF glass, specimens exhibited slip along a shear plane located at a 55°-70° angle from the compression loading axis. The shear angle for the SP specimens was slightly less, with an orientation of 50°-60° from the loading axis. Figure 6 shows respresentative shear planes for BF and SP specimens tested with hydraulic confinement (for confining pressures up to 250 MPa). The shear plane becomes more pronounced with increased confinement pressure.

Shear planes were also observed for confined sleeve specimens tested to higher confining pressures (~1 GPa max). The sectioned BF and SP specimens shown in Figure 7 are representative of the findings for the mechanical confinement tests. Note the dominant shear plane marked by the solid arrows, and the similarity in the shear angle for the sleeved specimens vs. the specimens tested in triaxial compression (see Figure 6). The maximum confining pressure for the sleeved specimens shown in Figure 7 was 870 MPa and 650 MPa for BF and SP glass, respectively. These observations indicate that the orientation of the shear failure is (i) independent of the confinement method (i.e., hydraulic vs. mechanical confinement), and (ii) independent of the confinement pressure for both glasses. It also appears independent of strain rate, based on limited high strain rate (~1 s^{-1}, ~1400 s^{-1}) test results for both glasses.

Both internal and surface damage were observed during post-test microscopy investigations. This was detected based on evaluation of several specimens at different viewing angles. Specimen BF-37 (Figure 7a) showed that the specimen curvature was maintained without

disruption of specimen fragments. Also, several specimens that were gold coated for SEM evaluation appeared more intact than identical uncoated specimens; see Ref. [26] for an illustration. The gold coating reduces the transparency of the glass, highlighting cracks that originated from or extend to the surface. Without the coating, it could not be determined whether the damage occurs on the surface or is internal.

SEM evaluations provided detailed views of the damage in the vicinity of the dominant shear plane for select predamaged specimens. For BF glass, a dusting of very fine (< 1 μm) particles was detected in the vicinity of the dominant shear plane. Fine particles are likely dislodged during axial loading as the specimen shifts to relieve the pressure. Higher magnification microscopy revealed the fine particles are actually aggregates of particles; few individual particles were observed. Generally, the aggregates were composed of rounded or spherical particles, as illustrated in Figure 8 for two representative BF specimens. Similar particle morphologies were also observed by Nie and Chen [14] in BF glass specimens following high strain rate compression tests conducted with a double pulse to simulate fracture and compaction. For BF specimens tested at a higher confining pressure, a hackle region was detected on some of the particles/aggregates. This is characteristic of brittle fracture, and is illustrated in Figure 8b at two different locations, marked by arrows. The two different orientations of the hackle lines indicate crack branching likely occurred.

The SP specimens exhibited greater fragmentation than the BF specimens following confinement testing. Loose particles were also detected in the vicinity of the dominant shear plane in predamaged SP glass. However, these particles were generally large and angular, as shown in Figure 9, with fewer round particles. The shape and size of the SP particles are readily compared with the BF particles in Figure 8; note the scale difference. The absence of very fine

particulates in the SP glass indicates less comminution than the BF glass, possibly due to the high density of pre-existing cracks. Whiskers were detected in some SP specimens following compression testing; see arrow in Figure 9a. These have also been reported by Bless [17] in soda-lime glass targets following high speed projectile impact. This phenomenon was not explored; further investigation is necessary to determine the growth kinetics.

Deformed and compacted glass particles were observed in the vicinity of the shear plane for some BF glass specimens. This is illustrated in Figure 10 for Specimen BF-83 following five compression load/reload cycles with mechanical confinement (max. confining pressure: ~395 MPa). The surface characteristics, and absence of loose particles, are evidence that particle sliding or rubbing occurred, resulting in compaction. A similar morphology was observed by Shockey, et al. [10,11] in the vicinity of the projectile following laboratory scale impact experiments on borosilicate glass.

For several of the BF specimens, it appears that the pressure was high enough for sintering of the particles to occur. This is illustrated in Figure 11 for a BF specimen tested with mechanical confinement at a strain rate of 2 s^{-1}; the maximum hydrostatic pressure in the specimen approached 2.0 GPa. At lower magnifications (Figure 11a), the compacted region shows individual particles. The compacted particles appear sintered when viewed at higher magnifications (Figure 11b). Compacted regions were not observed for SP glass following similar testing. For SP glass, the pressure is relieved with extension of pre-existing cracks and shear plane formation.

5.2 Damage Mechanism

Optical and SEM findings were compared to the mechanical response data, and used to support a hypothesis for the damage mechanism and continued load carrying capability of predamaged glass, as shown in Figure 3. Pressure buildup in the confined specimen, resulting from axial loading, causes movement and shifting within the glass specimen to relieve the pressure. This results in dislodgement of glass particles, as shown in Figures 8 and 9 for BF and SP glass, respectively. Damage likely initiates at dominant flaws (e.g., pre-existing cracks due to the thermal shock treatment); propagation proceeds with continued loading. The different orientations of the hackle regions, shown in Figure 8b, imply that damage propagation proceeds in different planes and directions. Eventually, separate damage regions link together. Initial failure occurs by slippage along a dominant shear plane, as shown in Figures 6 and 7, when the specimen can no longer support the maximum applied load. Subsequent loading of the confined specimen after formation of the dominant shear plane causes further shifting of the particles and fragments, and the creation of secondary damage regions and additional shear planes as illustrated in Figure 7.

Shifting of the glass material during axial loading requires movement of particles within the confined specimen. As the axial load is increased, the particles attempt to slide over each other. This requires considerable activation energy, based on the observed particle morphologies (see Figures 8 and 9). Initial movement is limited by frictional resistance between the particles. With continued loading, and increased axial stress, some particle sliding occurs. Movement becomes easier as particle compaction occurs and the particles are smoothed. Particle sintering, as shown in Figure 11, may occur with continued pressurization if high enough pressures are reached. Particle compaction and/or sintering result in decreased frictional resistance. Hence, the stress

required for particle motion decreases. Sliding of adjacent surfaces occurs more readily. The compacted zones detected (see Figures 10 and 11) provide evidence for operation of this phenomenon. Frictional resistance, followed by easy sliding of the particles past each other, likely accounts for the stress variations observed in the axial stress-strain curves in Figure 3. When the particle surfaces have been sufficiently smoothed due to sliding, this mechanism disappears and a relatively constant stress level is maintained.

At the outset of this section, the residual strength difference, shown in Figure 5, was indirectly attributed to compositional differences between the two glasses. The 0.5 GPa strength difference is rather large considering that the predamaged glasses demonstrate similar performance at hydrostatic pressures less than 1 GPa. The SEM post-test evaluations highlighted differences in the morphology of the particles. The inherent difference in the resultant particle shape following deformation is related to the specific glass composition. However, the extent of particle movement and sliding also contributes to the mechanical response. It is thought that this mechanical phenomenon also contributes to the observed difference in the strength cap. Material movement occurs more readily in SP glass owing to the angular, but plate-like particles. Confinement keeps the cracks from opening so that the angular particles cannot orient randomly. Rather, there is a tendency for the plate-like particles to stay oriented for preferential sliding. Sliding and shifting of particles is more restricted in BF glass owing to the spherical shape of the particles and larger size of the aggregates, observed in the vicinity of the shear plane in the BF specimens evaluated.

Continued loading of the confined glass specimens results in secondary damage regions, removed from the dominant shear plane. These regions are characterized by additional cracking and fragmentation, and were detected in both glasses. Primary and secondary damage regions

are illustrated in Figure 7a for BF glass. The dominant shear plane is marked by the solid arrow; the dashed arrow highlights the secondary damage region. Secondary damage regions were more prevalent in specimens tested at higher confining pressures.

More extensive damage was observed for specimens exposed to multiple loading cycles. For the triaxial tests, load cycling was performed after the thermal shock procedure to "comminute" the glass prior to testing. For some of the mechanical confinement tests at low strain rates, specimens were exposed to multiple load cycles. An increase in the extent of specimen damage with load cycling was first observed for BF glass based on a series of interrupted tests with increasing number of load cycles and load magnitude [18,19]. Further evaluations confirmed an increase in the number of shear planes formed due to multiple load cycling. These are illustrated in Figure 13 for a BF specimen following ten load/reload cycles with mechanical confinement.

6.0 Summary

Compression test results with confinement showed very different behavior for intact vs. predamaged Borofloat (BF) and Starphire (SP) glass. Both *intact* glasses failed suddenly upon loading. Observed variability in failure stress and strain of the intact glass is attributed to flaw sensitivity in these materials. *Predamaged* glass, both BF and SP, exhibited a linear axial stress-strain response with initial loading, though the moduli were less than the corresponding intact glass. Both predamaged glasses exhibited a strength drop after initial failure, but maintained a load carrying capability. The residual strength (i.e., strength cap) is approximately 2.1 GPa and 1.6 GPa for BF and SP glasses, respectively.

Post-test optical and electron microscopy findings were compared to the mechanical response data, and used to support a hypothesis for the damage mechanism. The damage development process likely progresses from dislodgement of glass particles to shifting/ movement of glass particles and overcoming frictional resistance. The observed differences in particle morphology between the two glasses are attributed to compositional differences. The extent of particle movement and sliding likely contributes to the stress variations in the axial stress-strain curve and the observed difference in the strength cap of the two glasses.

Damage initiates at dominant flaws (e.g., pre-existing cracks due to the thermal shock treatment). Damage propagation proceeds with continued loading and resultant linkage of the damage regions. Initial failure occurs by slippage along a dominant shear plane when the specimen can no longer support the maximum applied load. The orientation of the shear plane differed slightly for the two glasses: 55°-70° angle for BF vs. 50°-60° for SP. This orientation occurred independent of the confinement pressure and strain rate. Subsequent loading of the confined specimen after formation of the dominant shear plane causes further shifting of the particles and fragments, and the creation of secondary damage regions and additional shear planes.

7.0 Acknowledgements

The authors gratefully acknowledge the financial support of the US Army for this work. Dr. Doug Templeton and Mr. Rick Rickert of TARDEC are acknowledged for their technical and administrative support. Appreciation is also extended to Mr. Parimel Patel (US Army Research Laboratory) for providing the glass specimens tested early in this program, and for ultrasonic

measurements on both glasses. Mr. Art Nicholls (SwRI) is acknowledged for his skillful assistance with confined compression testing, and predamaging the test specimens.

8.0 References

1. J. Lankford, C.E. Anderson, Jr., A.J. Nagy, J.D. Walker, A.E. Nicholls, R.A. Page, "Inelastic Response of Confined Aluminum Oxide under Dynamic Loading Conditions", *J. Materials Science*, **33**(6): 1619–1625, 1998.

2. S.C. Desai and H.J. Siriwardane, ***Constitutive Laws for Engineering Materials with Emphasis on Geologic Materials***, Prentice-Hall, Englewood Cliffs, NJ, 1984.

3. T. J. Holmquist, G.R. Johnson, "A Computational Constitutive Model for Glass Subjected to Large Strains, High Strain Rates and High Pressures", *J. Appl. Mech.*, in publication, 2011.

4. D.R. Curran, D.A. Shockey and J.W. Simons, "Mesomechanical Constitutive Relations for Glass and Ceramic Armor", in ***Advances in Ceramic Armor IV,*** Ceramic Engineering and Science Proc., *32nd Int. Conf. on Advanced Ceramics and Composites*, edited by L. Prokurat-Franks, **29**(6): 3-13, Wiley, 2008.

5. D. Curran, "Mesomechanical Modeling of Fracture", ***Shock Compression of Condensed Matter – 2009***, edited by M.L. Elert, W.T. Buttler, M.D. Furnish, W.W. Anderson and W.G. Proud, CP1195, AIP, pp 3-10, 2009.

6. C. Lai, X Sun, and D.W. Templeton, "Analyses of Various Damage Mechanisms in Transparent Armor Subject to Projectile Impact", in ***Advances in Ceramic Armor V***, *Proc. of the 33rd Int. Conf. on Advanced Ceramics and Composites*, edited by J.J. Swab, **30**(5): 205-212, Wiley, 2009.

7. P. Forquin and F. Hild, "A Probabilistic Damage Model of the Dynamic Fragmentation Process in Brittle Materials", *Advances in Applied Mechanics*, **44**: 1-72, 2010.

8. K. A. Dannemann, S. Chocron, A. E. Nicholls, J. D. Walker, and C. E. Anderson, Jr., "Compression Testing and Response of SiC-N Ceramics: Intact, Damaged and Powder," ***Advances in Ceramic Armor***, Ceramic Engineering and Science, *Proc., 29th Int. Conf. on Advanced Ceramics and Composites*, edited by J.J. Swab, **26**(7): 109-116; Wiley, 2005.

9. T.J. Holmquist and G.R. Johnson, "The Failed Strength of Ceramics Subjected to High-Velocity Impact", *J. Appl. Physics*, **104**, 013533, 2008.

10. D.A. Shockey, J.W. Simons, and D.R. Curran, "The Damage Mechanism Route to Better Armor Materials", *Int. J. Appl. Ceram. Technol.*, **7**(5): 566–573, 2010.

11. D. A. Shockey, D. Bergmannshoff, D. R. Curran, and J. W. Simons "Physics of Glass Failure during Rod Penetration," ***Advances in Ceramic Armor IV***, Ceramic Engineering and Science Proc., *32nd Int. Conf. on Advanced Ceramics and Composites*, edited by L. Prokurat-Franks, **29**(6): 23-32, Wiley, 2008.

12. X. Nie, W.W. Chen, X. Sun, D.W. Templeton, "Dynamic Failure of Borosilicate Glass Under Compression/Shear Loading Experiments", *J. Am. Ceram. Soc.*, **90**(8): 2556–2562, 2007.

13. H. Luo and W. Chen, "Dynamic Compressive Response of Intact and Damaged AD995 Alumina", *Int. J. Appl. Ceram. Technol.*, **1**(3): 254–269, 2004.

14 X. Nie and W. Chen, "Temperature and Confinement Pressure Effects on Dynamic Response of Damaged Borosilicate Glass", American Ceramic Society, *35th Int. Conf. on Advanced Ceramics and Composites*, Daytona Beach, FL 2011.

15. A. A. Wereszczak, K. E. Johanns, T. P. Kirkland, C. E. Anderson Jr., T. Behner, P. Patel, and D. Templeton, ''Strength and Contact Damage Responses in a Soda–Lime-Silicate and a Borosilicate Glass''; Paper FP-05, *25th Army Science Conference*, Orlando, FL, November 27–30, 2006.

16. X. Nie, W. Chen., A.A. Wereszczak., D.W. Templeton, "Effects of Loading Rates and Surface Conditions on Flexural Strength of Borosilicate Glass", *J. Am. Ceram. Soc*, **92**(6): 1287-1295, 2009.

17. S. Bless and T. Chen, "Impact Damage in Layered Glass", *Int. J. Fracture*, **162**(1-2): 151-158, 2010.

18. K. A. Dannemann, A.E. Nicholls, C.E. Anderson, Jr., S.Chocron, J.D. Walker, "Response and Characterization of Confined Borosilicate Glass: Intact and Damaged", ***Advances in Ceramic Armor II***: *Ceramic Engineering and Science Proceedings*, edited by A. Wereszczak, E. Lara-Curzio, L. Prokurat Franks, **27**(7): 119-130, Wiley, 2006.

19. K.A. Dannemann, S. Chocron, A.E. Nicholls and C.E. Anderson, Jr., "Compressive Damage Development in Confined Borosilicate Glass", *Materials Science and Engineering: A*, **478**: 340-350, 2008.

20. P. Patel, M. Motyka, US Army Research Laboratory, Aberdeen, MD, personal communication, Sept. 2005.

21. ASTM E494, "Technique for Measuring Ultrasonic Velocity in Materials", July 2001.

22. Schott Glass, Borofloat 33 Thermal Properties datasheet http://www.us.schott.com/borofloat/ english/attribute/thermic/index.html.

23. Starphire Manufacturer Data Sheet – PPG Industries, Inc. http://www.jnsglass.com/pdf/Starphire.pdf

24. P. Forquin, A. Arias, and R. Zaera, ''An Experimental Method of Measuring the Confined Compression Strength of High-Performance Concretes to Analyse Their Ballistic Behaviour,'' *J. Phys. IV*, **134:** 629–34, 2006.

25. S. Chocron, C.E. Anderson, A.E. Nicholls and K.A. Dannemann, "Characterization of Confined Intact and Damaged Borosilicate Glass", *J. Amer. Ceram. Soc.*, **93**(10): 3390-3398, 2010.

26. S. Chocron, C.E. Anderson, A.E. Nicholls and K.A. Dannemann, "Characterization of Confined Intact and Damaged Soda-Lime Glass", *J. Amer. Ceram. Soc.*, submitted, 2011.

27. S. Bless, "Using DOP Tests to Evaluate Ballistic Performance of Transparent Material", American Ceramic Society, *35th Int. Conf. on Advanced Ceramics and Composites*, Daytona Beach, FL 2011.

LIST OF FIGURES

LIST OF FIGURES (cont'd)

LIST OF FIGURES (cont'd)

Table 1. Approximate Composition* of Borofloat® and Starphire® Glass [20]

Material	SiO_2	Na_2O	CaO	B_2O_3	Al_2O_3	MgO	K_2O	Fe_2O_3
Borofloat ®33	80.54	3.54	0.02	12.70	2.54	<0.01	0.64	0.015
Starphire ®	73.23	14.71	10.28	--	1.45	0.08	0.01	0.008

* Values listed for each glass are normalized weight percentages, averaged from four separate analyses.

Table 2. Properties of Borofloat® and Starphire® Glass [20]

	Borofloat® 33	Starphire®
Density (g/cc)	2.23	2.50
Elastic Modulus (GPa)	62.2	72.1
Shear Modulus (GPa)	26.0	29.5
Poisson's Ratio	0.195	0.222
Longitudinal Sound Speed, c_L (m/s)	5550	5750
Shear Wave Speed, c_S (m/s)	3416	3440
Linear Coefficient of Thermal Expansion*, α_L ($°C^{-1}$)	3.25×10^{-6} [22]	9.28×10^{-6} [23]

* from 20°C to 300°C

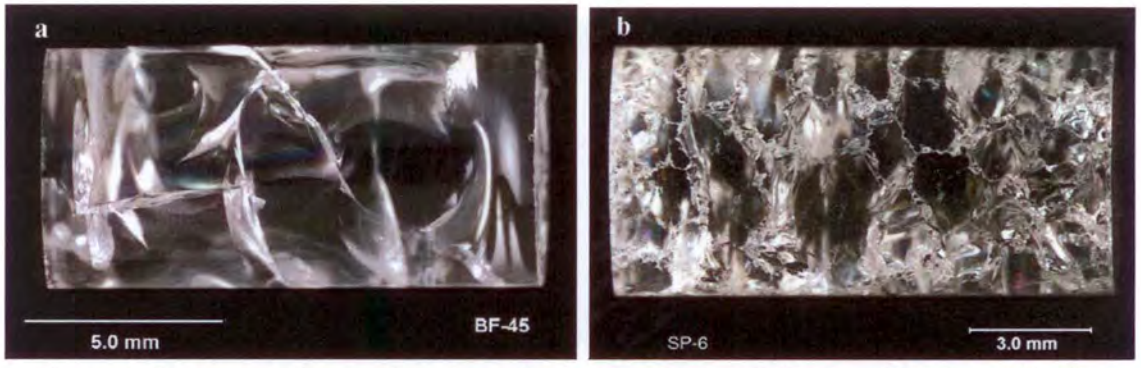

Figure 1. Representative crack patterns for (a) Borofloat and (b) Starphire glass following a thermal shock treatment. Photos illustrate the side view of pre-damaged specimens prior to testing.

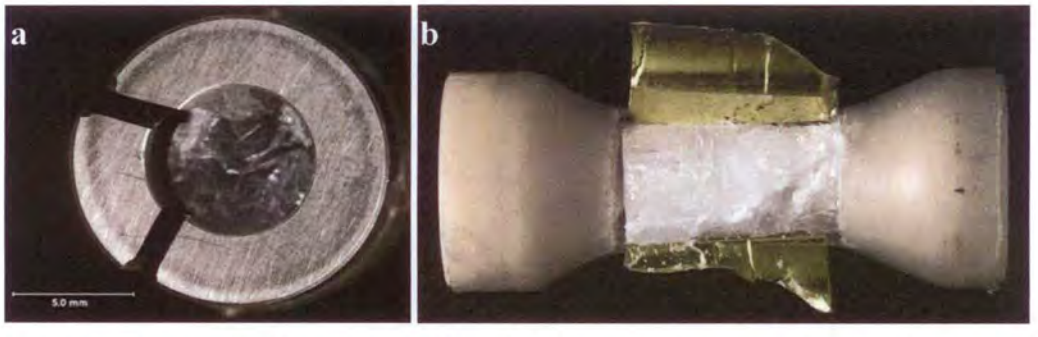

Figure 2. Removal of the confining sleeve/holder was necessary to view in-situ damage following compression testing of. (a) Confined sleeve specimen – end view, (b) Triaxial compression specimen (BF-52) – lengthwise view.

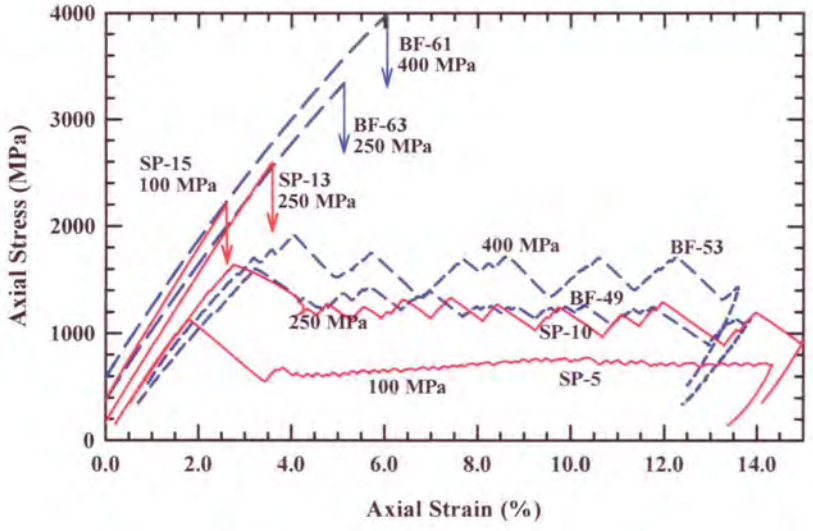

Figure 3. Axial stress-strain response of intact and pre-damaged Borofloat (BF curves) and Starphire (SP curves) specimens tested in triaxial compression.

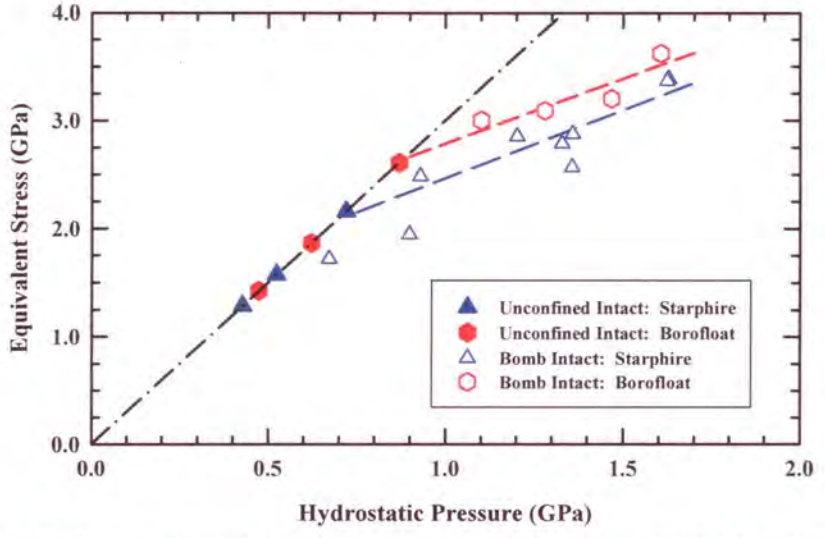

Figure 4. Equivalent stress vs. hydrostatic pressure comparison plot for intact Borofloat and Starphire glass specimens for data obtained from confined (bomb intact) and unconfined tests [26].

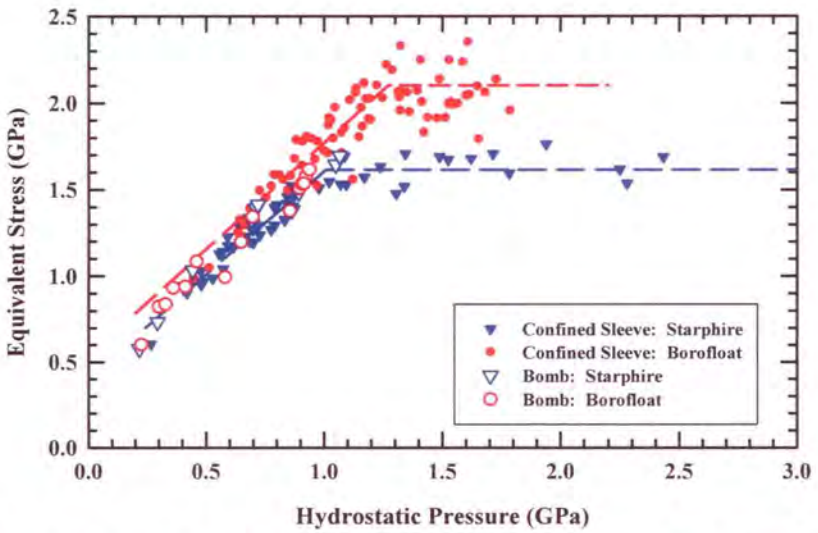

Figure 5. Equivalent stress vs. hydrostatic pressure comparison plot obtained from confined compression test data on pre-damaged Borofloat and Starphire glass specimens [26].

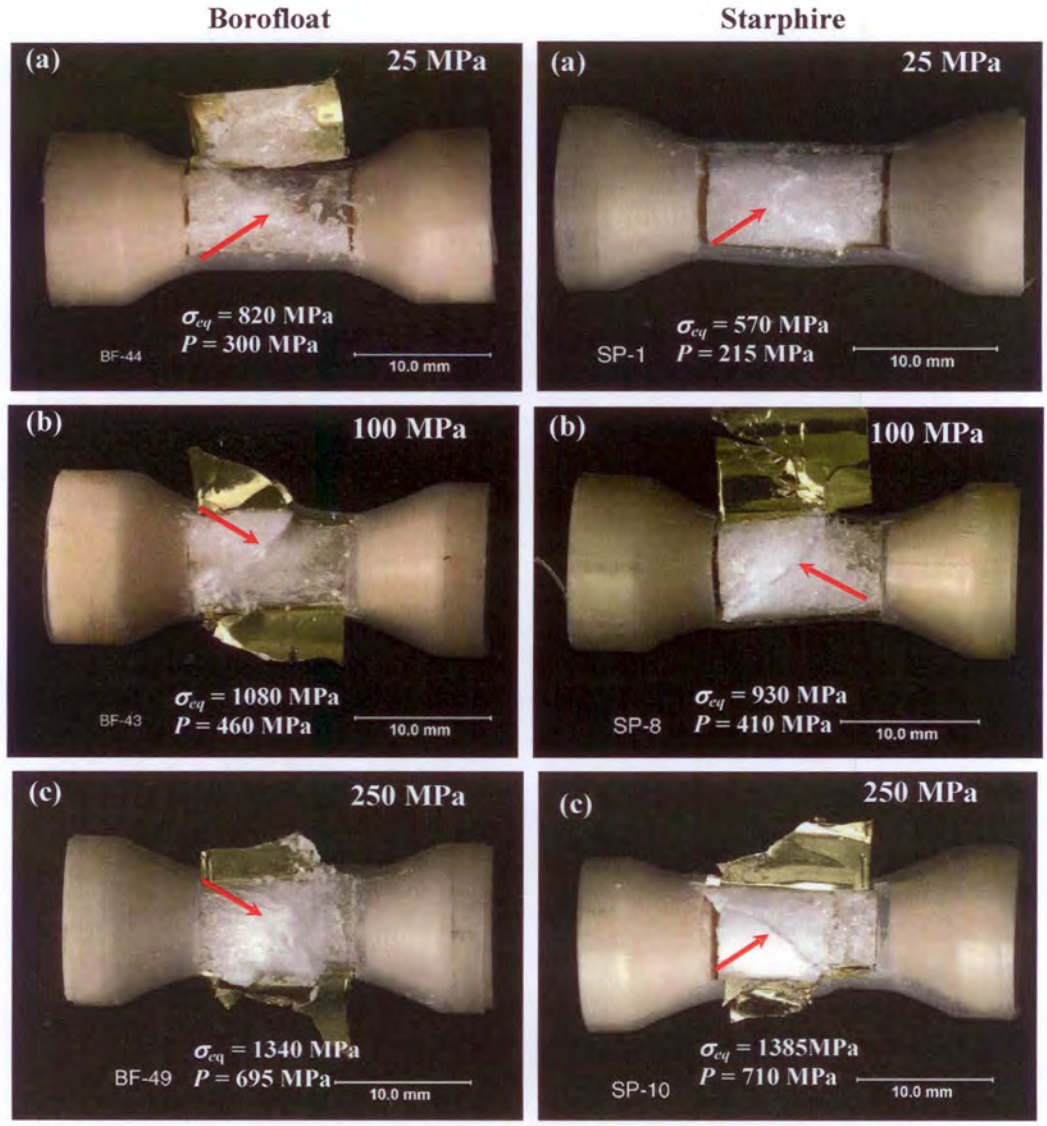

Figure 6. Pre-damaged Borofloat and Starphire specimens following monotonic loading with hydraulic confining pressures of (a) 25 MPa, (b) 100 MPa, (c) 250 MPa. The dominant shear plane, marked by an arrow in each photo, is oriented 55-70° from the loading axis for Borofloat, and 50-60° for Starphire. The equivalent stress and hydrostatic pressure (at bottom) correspond to the data plotted in Figure 5.

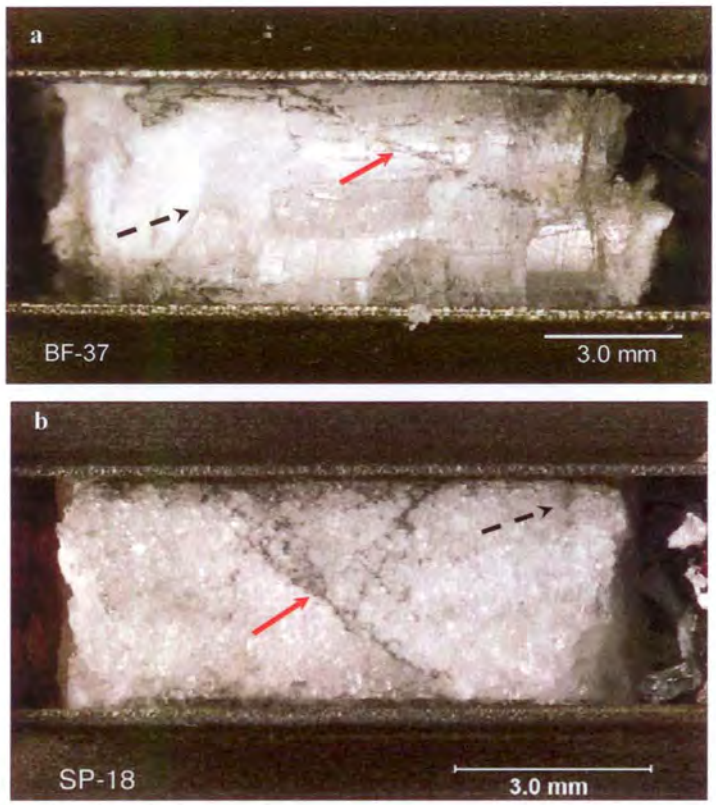

Figure 7. Dominant shear plane (solid arrow) and secondary damage regions (dashed arrow) formed during confined sleeve testing of:

a) Borofloat (BF-37): Max σ_{eq} = 2210 MPa, Max $\widetilde{\sigma}_r$ = 870 MPa; Max P = 1580 MPa.

b) Starphire (SP-18): Max σ_{eq} = 1530 MPa, Max $\widetilde{\sigma}_r$ = 650 MPa; Max P = 1150 MPa.

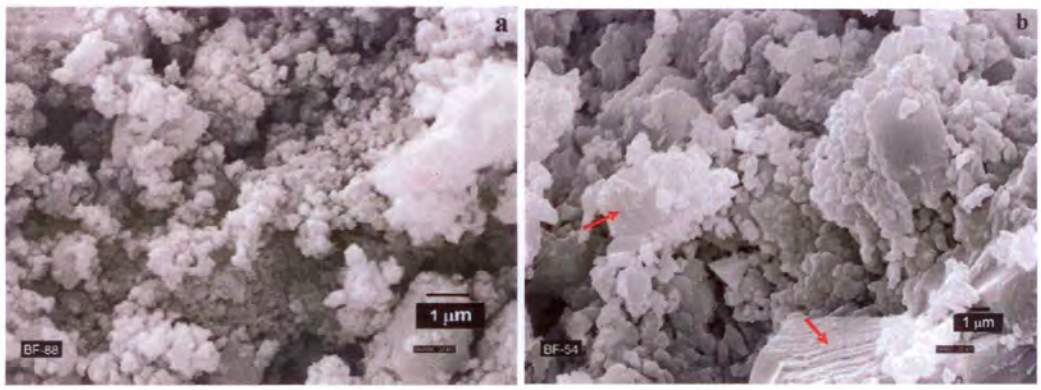

Figure 8. Rounded particles in the vicinity of the shear plane for Borofloat specimens tested with hydraulic confinement. (a) Specimen BF-88: $\widetilde{\sigma}_r$ = 250 MPa, max P = 730 MPa; (b) Specimen BF-54: $\widetilde{\sigma}_r$ = 400 MPa, max P = 905 MPa.

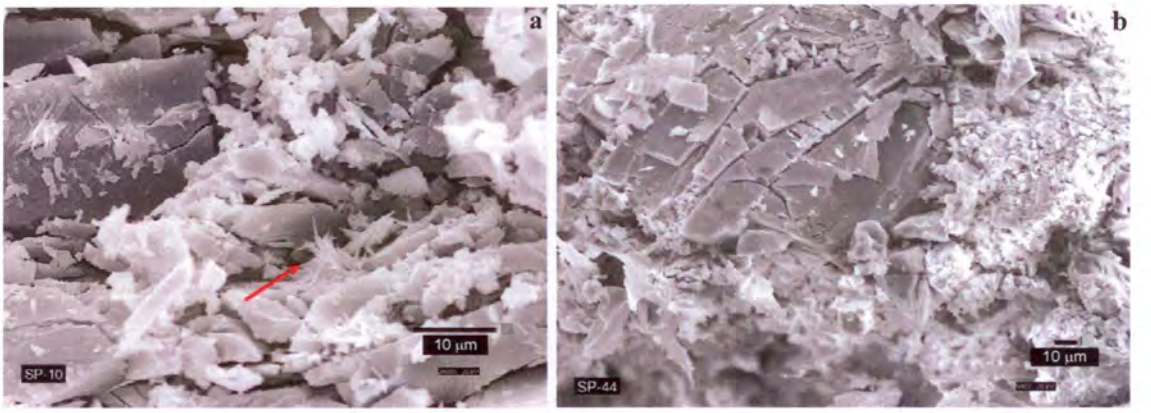

Figure 9. Angular particles in the vicinity of the shear plane for Starphire specimens tested with hydraulic confinement. (a) Specimen SP-10: $\widetilde{\sigma}_r = 250$ MPa, max $P = 710$ MPa; (b) Specimen SP-44: $\widetilde{\sigma}_r = 500$ MPa, max $P = 1100$ MPa.

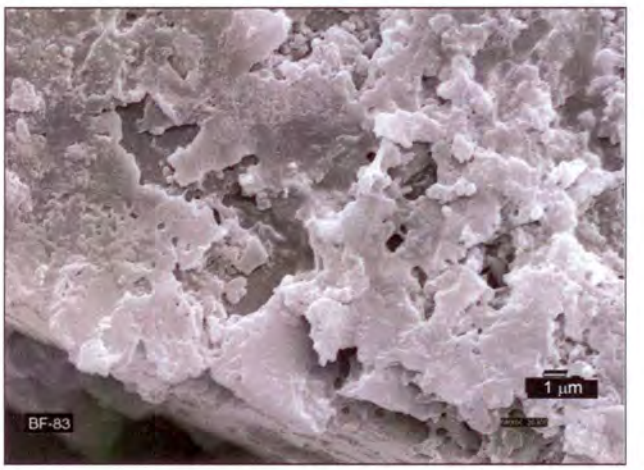

Figure 10. Compacted particles in the vicinity of the shear plane for a Borofloat specimen, following quasistatic testing with mechanical confinement and a maximum confining pressure of 395 MPa. Five load/unload cycles were applied (Max $\sigma_{eq} = 2120$ MPa, Max $P = 1100$ MPa).

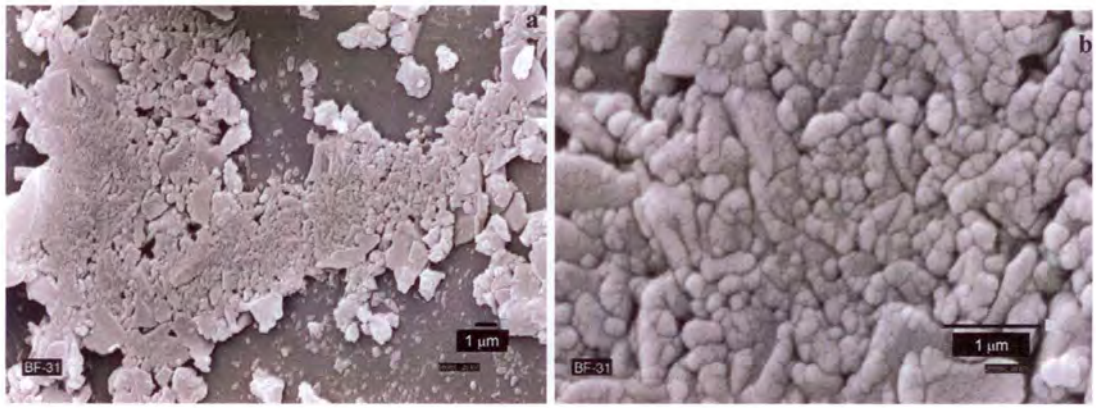

Figure 11. Compacted and sintered regions in Borofloat glass following compression testing (strain rate = 2 s^{-1}, 1 cycle only) with mechanical confinement. The micrograph on the right is a magnified view of Figure 11a. Max σ_{eq} = 2200 MPa, $\tilde{\sigma}_r$ = 1245 MPa; Max P = 1980 MPa

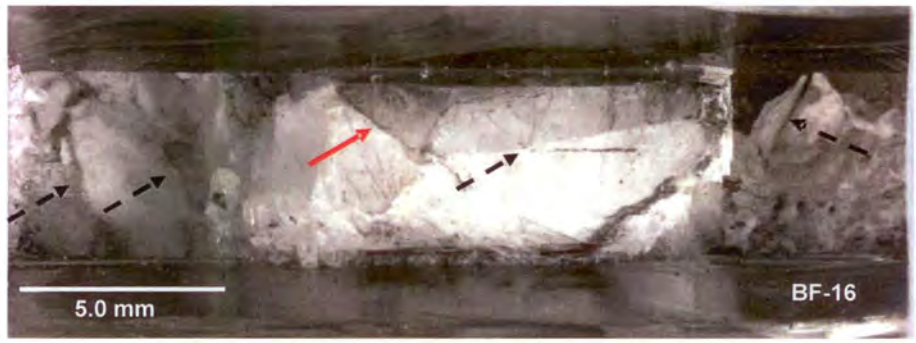

Figure 12. Multiple shear planes in a pre-damaged Borofloat specimen following compression testing with mechanical confinement ($\tilde{\sigma}_r$ = 100 MPa) and ten load/reload cycles. The solid arrow highlights the dominant shear plane; secondary shear planes are marked with dashed arrows.